A Cumulus Parameterization Including Mass Fluxes, Vertical Momentum Dynamics, and Mesoscale Effects

LEO J. DONNER

Geophysical Fluid Dynamics Laboratory/NOAA, Princeton University, Princeton, New Jersey

(Manuscript received 27 January 1992, in final form 1 June 1992)

ABSTRACT

A formulation for parameterizing cumulus convection, which treats cumulus vertical momentum dynamics and mass fluxes consistently, is presented. This approach predicts the penetrative extent of cumulus updrafts on the basis of their vertical momentum and provides a basis for treating cumulus microphysics using formulations that depend on vertical velocity. Treatments for cumulus microphysics are essential if the water budgets of convective systems are to be evaluated for treating mesoscale stratiform processes associated with convection, which are important for radiative interactions influencing climate.

The water budget (both condensed and vapor) of the cumulus updrafts is used to drive a semi-empirical parameterization for the large-scale effects of the mesoscale circulations associated with deep convection. The parameterization for mesoscale effects invokes mesoscale ascent to redistribute vertically water detrained at the tops of the cumulus updrafts. The local cooling associated with this mesoscale ascent is probably larger than radiative heating of the mesoscale anvil clouds, and the mesoscale ascent may be in part a response to such radiative heating.

The parameterization was applied to two tropical thermodynamic profiles whose diagnosed forcing by convective systems differed significantly. A spectrum of cumulus updrafts was allowed. The deepest of the updrafts penetrated the upper troposphere, while the shallower updrafts penetrated into the region of the mesoscale anvil. The relative numbers of cumulus updrafts of characteristic vertical velocities comprising the parameterized ensemble corresponded well with available observations. However, the large-scale heating produced by the ensemble without mesoscale circulations was concentrated at lower heights than observed or was characterized by excessive peak magnitudes. Also, an unobserved large-scale source of water vapor was produced in the middle troposphere. When the parameterization for mesoscale effects was added, the large-scale thermal and moisture forcing predicted by the parameterization agreed well with observations for both cases.

The significance of mesoscale processes, some of which may depend in part on radiative forcing, suggests that future cumulus parameterization development will need to treat some radiative processes. Further, the long time scale of the mesoscale processes relative to that of the cumulus cells indicates a possible requirement for carrying some characteristics of the convective system in time as cumulus parameterizations are incorporated in large-scale models whose resolutions remain too large to capture explicitly the mesoscale processes.

1. Introduction

Parameterizing the effects of cumulus convection on the larger-scale flows in which it is embedded remains among the key unresolved challenges to modeling the atmospheric general circulation for climate simulation and numerical weather prediction. Cumulus convection forces large-scale flows by generating and transporting heat, moisture, and momentum. Its roles in transporting chemical tracers and possibly in providing reaction vessels for them are only on the verge of quantitative understanding.

Cumulus parameterizations have developed around several hypotheses relating the aggregate characteristics of a cumulus ensemble to its large-scale environment. Such hypotheses include 1) linkage between moisture convergence and the intensity of convection and 2) equilibria manifested either in temperature and moisture profiles or in the rates at which convective stabilization balances large-scale destabilization. Parameterizations using moisture convergence as a key indicator of the intensity of convection were introduced by Kuo (1965). Adjustment to an equilibrium thermodynamic profile is a key characteristic of the parameterizations of Manabe et al. (1965) and Betts (1986), while the parameterizations of Arakawa and Schubert (1974) and Fritsch and Chappell (1980) depend on hypotheses governing the release and generation of buoyant cumulus energy. Although these hypotheses differ considerably in technique, some common threads link their underlying physical concepts. For example, the rate of low-level convergence (and, thereby, moisture convergence) will often be a significant term contributing to the rate of large-scale destabilization. Thus, Kuo parameterizations embody some

Corresponding author address: Dr. Leo J. Donner, Geophysical Fluid Dynamics Laboratory/NOAA, Princeton University, Forrestal Campus, US Route 1, P.O. Box 308, Princeton, NJ 08542.

elements of the equilibria associated with other cumulus parameterizations.

As noted above, some cumulus parameterizations simply adjust temperature or moisture profiles to account for the effects of convection. Parameterizations that attempt to represent the physical processes associated with convection more explicitly require simple cumulus models. Generally, the properties of the modeled cumuli that are important for the parameterization depend on the large-scale flow in which the clouds form. Early cumulus parameterizations conceptualized the convective ensemble as consisting of updrafts, possibly all identical for a given large-scale flow (e.g., Anthes 1977) or possibly varying in important characteristics (e.g., Arakawa and Schubert 1974). More recent work has emphasized that other processes associated with convection modify significantly the basic interaction between updrafts and the large scale. Among these processes are convective-scale downdrafts (Johnson 1976; Cheng 1989) and mesoscale updrafts and downdrafts (Leary and Houze 1980; Johnson and Young 1983; Cheng and Yanai 1989). Convective-scale downdrafts have recently been included in cumulus parameterizations (Tiedtke 1989) for general circulation models (GCMs). Fritsch and Chappell (1980) included convective-scale downdrafts in their cumulus parameterization for mesoscale models, and Molinari and Corsetti (1985) developed a parameterization in which the effects of both mesoscale and convective-scale downdrafts were represented.

There are two primary purposes for this paper: 1) to present a parameterization for the interactions between cumulus updrafts and their large-scale flows and 2) to present a method for parameterizing the modifications to this basic interaction by mesoscale circulations driven by convection. The parameterization calculates distributions of both cumulus vertical momentum and cumulus mass flux explicitly, in contrast to those parameterizations generally referred to as *mass flux* parameterizations. Mass-flux parameterizations (e.g., Arakawa and Schubert 1974; Tiedtke 1989) also invoke a cloud (or cloud ensemble) model; these parameterizations calculate the cumulus mass flux but not the vertical momentum budget. Evaluating the impact of liquid water loading on cumulus mass flux requires introducing the vertical momentum dynamics of the cumulus elements, and even simple representations of cumulus microphysics depend partly on the distribution of cumulus vertical momentum. Therefore, treating jointly cumulus mass fluxes and cumulus vertical momentum dynamics is useful for parameterizing the interaction between the cumulus updrafts and the large-scale flow. Moreover, such an approach also facilitates calculating mesoscale effects associated with the basic cumulus updrafts, because knowledge of both the vertical distribution of condensation and the microphysical properties provides the proportion of condensed water that actually precipitates directly from the cumulus cells. The remaining condensed water is available to participate in such processes as evaporatively driven downdrafts or mesoscale anvil clouds, which modify significantly the basic interaction between cumulus updrafts and the large-scale flow, as noted before. Leary and Houze (1980) found that the ratio of convective rainfall to convective condensation was an important parameter in characterizing the mesoscale effects of the convective systems they studied. Their results will be used in conjunction with the water budget of the cumulus updrafts in the parameterization to develop a semi-empirical modification to represent the effects of mesoscale circulations and convective downdrafts. It appears likely that radiative forcing involving the mesoscale anvil cloud is important to the vertical structure of these mesoscale effects.

Section 2 of the paper describes the parameterization for interactions between large-scale flows and cumulus updrafts and the modifications produced by mesoscale effects. Section 3 presents applications of the parameterization to composite soundings observed in the east Atlantic during GATE (GARP [Global Atmospheric Research Program] Atlantic Tropical Experiment) and in the west Pacific at the Kwajalein, Eniwetok, and Ponape (KEP) triangle. The vertical structures of forcing by cumulus convection diagnosed from observations differed in the two regions. Concluding remarks are presented in section 4.

2. Parameterization

The effects of cumulus convection on the large-scale fields of potential temperature $\bar{\theta}$ and water vapor mixing ratio $\bar{q}$ are obtained by decomposing these fields into large-scale and smaller-scale components and then averaging the thermodynamic and moisture equations over the large scale. In isobaric coordinates,

$$\frac{d\bar{\theta}}{dt} - \frac{\pi \overline{Q_r}^e}{c_p} - \frac{\pi \sum_{i=1}^{6} L_i \overline{\Upsilon_i}^e}{c_p} = \frac{\pi \overline{Q_r}^*}{c_p} + \frac{\pi \sum_{i=1}^{6} L_i \overline{\Upsilon_i}^*}{c_p} - \frac{\partial \overline{\omega'\theta'}}{\partial p} - \nabla \cdot \overline{\mathbf{v}'\theta'}, \quad (1)$$

$$\frac{d\bar{q}}{dt} + \sum_{i=1}^{4} \frac{|L_i|}{L_i} \overline{\Upsilon_i}^e = -\sum_{i=1}^{4} \frac{|L_i|}{L_i} \overline{\Upsilon_i}^* - \frac{\partial \overline{\omega'q'}}{\partial p} - \nabla \cdot \overline{\mathbf{v}'q'}. \quad (2)$$

Here Q_r denotes radiative heating, c_p specific heat at constant pressure, and $\pi = (p_0/p)^{R_d/c_p}$, where $p_0 = 100$ kPa, and R_d is the gas constant for dry air. The summations represent phase transformations. The latent heat of vaporization is given by L_1, while L_3 is the latent heat of sublimation and L_5 is the latent heat of fusion. For the reverse processes,

$$L_2 = -L_1, \quad L_4 = -L_3, \quad L_6 = -L_5.$$

The phase transformations (all expressed as positive semidefinite quantities) include Υ_1, condensation; Υ_2, evaporation; Υ_3, deposition (from water vapor to ice); Υ_4, sublimation; Υ_5, freezing; and Υ_6, melting. The horizontal velocity vector is $\mathbf{v}$, and the vertical pressure velocity is ω. Cloud properties and those of their environment are denoted by asterisks and superscripts e, respectively, while primes denote departures from the large-scale average. The horizontal eddy fluxes will subsequently be neglected, as discussed in Anthes (1977). Equations (1) and (2) then show that large-scale forcing by cumulus convection requires evaluating fluxes and phase transformations. Radiative effects, $\overline{Q_r}^*$, could be calculated once the optical properties of the convective system are established, but this topic will not be considered here. In addition, radiative forcing could play a role in the evolution of the convective system itself, in which case radiative heating might not be apparent as such on the large scale. Allusion to a possible mechanism of this nature will appear in section 2b.

Equations similar to (1) and (2) could also be formulated for horizontal momentum, potential vorticity, and chemical tracers. Although not the subject of the present paper, these interactions between convection and large-scale flows are also likely to be important.

a. *Cumulus updrafts*

A formulation for the terms on the right sides of (1) and (2) when cumulus updrafts interact with their large-scale flow will be developed first. Modifications associated with mesoscale anvil clouds and convective downdrafts will be presented later. The parameterization will emphasize deep convection.

Extending Kuo (1974) to multimodal cumulus ensembles, the vertical eddy transport of a property χ is given by

$$\overline{\omega'\chi'} = \sum_{i=1}^{N} (\overline{\omega'\chi'})_i, \tag{3}$$

where

$$(\overline{\omega'\chi'})_i = \frac{a_i \omega_i^{*\prime} \chi_i^{*\prime}}{1 - a_i},$$

where a_i is the fractional area occupied by cumulus clouds of the ith subensemble. ($1 - a_i$ is approximated as 1.) The ensemble is comprised of N such subensembles. Large-scale phase transformations due to cumulus convection are given by

$$\overline{\Upsilon_i}^* = \sum_{j=1}^{N} a_j \Upsilon_{i,j}^*, \tag{4}$$

where $\Upsilon_{i,j}^*$ is the rate of the ith phase transformation per unit mass in a cumulus updraft belonging to subensemble j.

Evaluating cumulus forcing of the large-scale flow in (1) and (2) requires T^*; the cumulus temperature, q^*, ω^*, a; and the rates of phase transformations in the cumulus updraft. [For notational clarity, the subscript i will now be dropped. This discussion applies separately to each subensemble, with aggregation proceeding according to (3) and (4).] Except for a, all are properties of the cumulus updraft. The product of ω^* and a is proportional to the cumulus mass flux.

The following three simultaneous differential equations with initial conditions at cloud base provide T^*, ω^*, and a. Since q^* is a function of T^* through saturation and the phase-transformation rates can be calculated once q^* and the vertical distribution of cumulus mass flux are known, the parameterization is described by

$$\frac{dT^*}{dz} = -\left\{\left(T_v^* + \frac{Lq^*}{R^*}\right)\frac{g}{c_p T^*} + \frac{1}{\rho^* a w^*}\frac{d(\rho^* a w^*)}{dz}\left[(T^* - \bar{T}) + \frac{L}{c_p}(q^* - \bar{q})\right]\right\}\left(1 + \frac{\epsilon L}{c_p p}\frac{de_s^*}{dT^*}\right)^{-1}, \tag{5}$$

$$\frac{d}{dz}\left(\frac{w^{*2}}{2}\right) = \frac{gB}{1+\alpha} - gQ_{lw} - \frac{1}{\rho^* a w^*}\frac{d(\rho^* a w^*)}{dz} w^{*2}, \tag{6}$$

$$\frac{1}{\rho^* a w^*}\frac{d(\rho^* a w^*)}{dz} = \frac{\beta\sqrt{a(p_b)}}{R(p_b)\sqrt{a}}. \tag{7}$$

Equation (5) is modified as described in the following if freezing of liquid water occurs. Notation introduced in (5)–(7) includes: T_v for virtual temperature,

$$R^* = R_d\left[1 + \left(\frac{1}{\epsilon} - 1\right)q^*\right]$$

for the cloud gas constant, g for the gravity constant, ρ for density, z for geometric height, ϵ for the ratio of the molecular weights of water to dry air, e_s for saturation vapor pressure, w for geometric vertical velocity, $B = (T_v^* - \overline{T_v}^e)/\overline{T_v}^e$ for buoyancy, $\alpha = 0.5$ for the virtual mass coefficient, Q_{lw} for the mixing ratio of cloud liquid water, R for cloud radius, and p_b for cloud-base pressure. The latent heat L takes the value L_1 if $T^* \geqslant 258$ K, and L_3 if $T^* < 258$ K. The expression on the left side of (7) defines an entrainment coefficient,

$$\mu = \frac{1}{\rho^* a w^*}\frac{d(\rho^* a w^*)}{dz}, \tag{8}$$

which is inversely proportional to R through β. The values for β are discussed later.

Note that (5)–(7) are coupled through the entrainment coefficient, which, when expanded using the chain rule, is a linear combination of dT^*/dz, dw^*/dz, and da/dz, since ρ can be expressed in terms of T_v and p using the equation of state.

When T^* falls to 258 K, freezing begins. The liquid water freezes linearly until T^* reaches 248 K (cf. Kreitzberg and Perkey 1976). Below 258 K, vapor is deposited to ice instead of liquid. Since some of the liquid at 258 K will fall out as precipitation while the parcel is rising and cooling to 248 K, not all of the liquid water at 258 K will actually freeze. The microphysical parameterization could be modified to take account of the ice phase explicitly to treat this situation, but instead, the simpler approach of not freezing a fraction of the liquid water equal to the observed cloud-average ratio of precipitation to condensation (0.48, from Leary and Houze 1980) is used. The product of the cumulus fractional area and the freezing rate in a cumulus cloud of subensemble i then yields $\overline{\Upsilon}_5^*$. Melting is discussed in the following.

The essential physics represented by Eq. (5), from Kuo and Raymond (1980), is conservation of the adiabatic equivalent potential temperature of the mass of cloud and entrained air as lifting, phase transformations, and lateral mixing occur. Equation (6) states that the vertical momentum of the cloud is changed by buoyancy (reduced by the virtual mass coefficient to take account of nonhydrostatic effects), liquid loading, and entrainment of low-momentum air from outside of the cloud (cf. Anthes 1977). The effects of entrainment on T^* and w^* in (5) and (6) can be derived by assuming adiabatic equivalent potential temperature or vertical velocity (with zero vertical velocity for air outside the cloud) mix conservatively during entrainment. While this is reasonable for adiabatic equivalent potential temperature, it is problematic for vertical velocity owing to the presence of pressure gradient forces. It is also unclear to what extent cloud entrainment proceeds by lateral mixing. Nonetheless, (5) and (6) provide a plausible and consistent, yet simple and one-dimensional, representation of both the dynamics and thermodynamics of cumulus clouds, which is still economical enough for use in cumulus parameterization. Equation (7) is simply the traditionally invoked inverse relationship between entrainment and radius (e.g., Simpson and Wiggert 1969) for a given cumulus subensemble, in which the number of cumulus clouds does not vary with height, enabling $R(p)$ to be expressed in terms of $a(p)$, $a(p_b)$, and $R(p_b)$. Kreitzberg and Perkey (1976) considered the interaction between a convective cloud governed by dynamics and thermodynamics similar to (5)–(7) and its large-scale environment.

At p_b, T^*, w^*, a, and R must be specified as initial values in order to solve the set (5)–(7). The vertical velocity at cloud base is set at 0.5 m s^{-1}; Simpson and Wiggert (1969) quoted results showing one-dimensional cloud models are not strongly sensitive to this choice. The cumulus fractional area at cloud base is evaluated through a closure for the cumulus parameterization relating the large-scale flow to the cumulus mass flux ($\rho^* a w^*$) at cloud base. As an example, in the calculations presented in section 3, the parameterization is closed using the observed precipitation rate; this precipitation rate, in turn, implies a mass flux at cloud base, through the microphysical parameterization (discussed in the following). In fully prognostic applications, the precipitation rate would be evaluated by using a closure assumption; such closures are components of cumulus parameterizations presently in use. Here $R(p_b)$ is treated using the procedure described in section 3a. The temperature at cloud base is evaluated by lifting a parcel from p_0 to the lifting condensation level (LCL).

In experiments with GATE data, it was found that a parcel assigned a vertical velocity of 0.5 m s^{-1} at the LCL was unable to reach the level of free convection (LFC), consistent with results presented by Thompson et al. (1979), which showed that 7.83 J kg^{-1} would be required for a parcel to reach the LFC. Although vertical velocities at cloud base sufficient to overcome this energy barrier are sometimes observed (Jorgensen and LeMone 1989), the following procedure has been adopted here. The parcel is lifted at the cloud-base vertical velocity until it becomes buoyant; that is, (6) is replaced by $w^* = w^*(p_b)$, while (5) and (7) still hold. The physical basis for this approach is the presence of mesoscale regions of intensified low-level convergence (such as gust fronts) (Houze and Betts 1981), unresolved by the large scale, which can lift parcels to their LFC. There is little theoretical basis for parameterizing such mesoscale convergence as a function of the large-scale flow at present; in a prognostic application, a limit would be imposed on the height of the LFC, along with the other criteria for the occurrence of deep cumulus convection. [Thompson et al. (1979) provide an observational basis for doing so.]

A simple treatment of cloud microphysics is used to evaluate Q_{lw}, $\overline{\Upsilon}_1^*$, and $\overline{\Upsilon}_3^*$. As summarized in Anthes (1977) and Kuo and Raymond (1980), cloud condensed water, Q_{lw}, consists of cloud water, Q_{cw}, and rainwater, Q_{rw}. As a cloud parcel is displaced a distance Δz, cloud water increases by condensation or deposition (depending on whether the temperature is above or below 258 K), $(\Delta Q_{cw})_{\text{cond}}$, and decreases by autoconversion of cloud water to rainwater, $(\Delta Q_{cw})_{\text{auto}}$, and by collection of cloud water by rainwater, $(\Delta Q_{cw})_{\text{coll}}$. The latter two processes increase rainwater; rainwater is decreased by fallout $(\Delta Q_{rw})_{\text{fall}}$:

$$\Delta Q_{cw} = (\Delta Q_{cw})_{\text{cond}} - (\Delta Q_{cw})_{\text{auto}} - (\Delta Q_{cw})_{\text{coll}}, \quad (9)$$

$$\Delta Q_{rw} = (\Delta Q_{cw})_{\text{auto}} + (\Delta Q_{cw})_{\text{coll}} - (\Delta Q_{rw})_{\text{fall}}. \quad (10)$$

Simple parametric expressions are provided in the cited references for $(\Delta Q_{cw})_{\text{auto}}$, $(\Delta Q_{cw})_{\text{coll}}$, and $(\Delta Q_{rw})_{\text{fall}}$; $(\Delta Q_{cw})_{\text{cond}}$ can be calculated by assuming the cloud

mixing ratio to be at its saturation value, with modifications to account for entrainment of environmental air. Several of the terms in (9) and (10) depend on w^*; the possibility of treating microphysics with this dependency is a key motivation for using (6) in the parameterization, instead of treating mass fluxes only.

The rate of condensation Υ_1^* (or deposition Υ_3^*) associated with (9) is given by $(\Delta Q_{cw})_{\text{cond}} w^*/\Delta z$. The integral $\int_{p_t}^{p_b} \overline{\Upsilon_1}^* dp$ (or $\int_{p_t}^{p_b} \overline{\Upsilon_3}^* dp$) measures the large-scale conversion of water vapor to condensate, and its product with the ratio

$$\frac{\sum_{i=1}^{M} (\Delta Q_{rw})_{\text{fall},i}}{\sum_{i=1}^{M} (\Delta Q_{cw})_{\text{cond},i}},$$

yields precipitation at the ground. (The number of vertical displacements Δz is M.) Unless liquid water is carried prognostically across time step in the large-scale model with which the parameterization is used, surface precipitation represents the net heating of the column due to cumulus convection. The difference between $\int_{p_t}^{p_b} (\overline{\Upsilon_1}^* + \overline{\Upsilon_3}^*) dp$ and the vapor removal by surface precipitation yields $\int_{p_t}^{p_b} (\overline{\Upsilon_2}^* + \overline{\Upsilon_4}^*) dp$. This evaporated (or sublimated) water could become involved in the formation of mesoscale anvil clouds before ultimately becoming water vapor. In order to parameterize cumulus towers in the absence of mesoscale effects, assumptions about the vertical distributions of $\overline{\Upsilon_2}^*$ and $\overline{\Upsilon_4}^*$ are required. For example, Arakawa and Schubert (1974) assumed that all evaporation for a cumulus element of given entrainment coefficient occurred at the level at which liquid water was detrained, that is, at the cloud top. In order to facilitate comparison of the parameterization with earlier cumulus parameterizations, $\overline{\Upsilon_2}^*$ will be taken as proportional to $\overline{\Upsilon_1}^*$, with sublimation and deposition behaving analogously. This assumption, which will be used to calculate forcing by cumulus ensembles for cases in which mesoscale effects are not included, results in a "net condensation" whose vertical distribution is determined by the distribution of cumulus latent heat release, as in Kuo (1974), Anthes (1977), Donner et al. (1982), and Donner (1986). Although implicitly adopted in these earlier studies, this assumption is physically problematic. (There is no reason to expect the processes governing evaporation to have the same vertical distribution as those for condensation.) However, since observational studies suggest that around 40% of the precipitation in tropical convective systems is actually due to mesoscale anvil clouds and not the convective updrafts themselves (Leary and Houze 1980), a more important issue centers around the means by which the associated mesoscale effects are treated. Such a treatment will be presented in section 2b, and this assumption on the vertical distributions of $\overline{\Upsilon_2}^*$ and $\overline{\Upsilon_4}^*$ will then no longer be required.

Finally, in the absence of mesoscale effects, $\int_{p_t}^{p_b} \overline{\Upsilon_6}^* dp$ is taken to be $\int_{p_t}^{p_b} (\overline{\Upsilon_3}^* + \overline{\Upsilon_5}^* - \overline{\Upsilon_4}^*) dp$. Between p_b and the pressure at which the cloud temperature reaches 273 K, $\overline{\Upsilon_6}^*$ is distributed uniformly. In the presence of mesoscale circulations, melting, like evaporation, will be treated differently.

b. Circulations outside cumulus updrafts

As noted before, a significant portion of the precipitation associated with convective systems is from mesoscale anvil clouds associated with the cumulus towers. The mechanisms that determine the precise nature of the mesoscale effects are quite complex and probably involve both dynamical and radiative processes. The view adopted here is that the mesoscale anvil clouds are largely driven by the cumulus updrafts, which supply water vapor and condensed water for them. A parameterization for mesoscale effects is presented, which is tied to the properties of the cumulus updrafts parameterized in the preceding subsection. Due to the complexity of the mesoscale effects, a semi-empirical approach is adopted, largely following Leary and Houze (1980), who diagnosed the moisture budget of a tropical convective system by relating precipitation in convective towers to other components of the convective moisture budget. Some components of this budget can be deduced directly from the parameterization for the cumulus updrafts, while others are taken from Leary and Houze (1980). Very little information is available on the vertical distribution of the various components of the moisture budget, and the parameterization of mesoscale effects was found to exhibit some sensitivity to choices thereof. This parameterization of mesoscale effects is intended to be only a rudimentary representation and should ideally be replaced by a more physically based approach as further knowledge is gained.

In Leary and Houze (1980), the water budget of a convective system consists of condensation in convective updrafts C_u, precipitation from convective updrafts R_c, evaporation of condensate from convective updrafts E_{ce}, evaporation in convective downdrafts E_{cd}, precipitation from mesoscale updrafts R_m, condensation in mesoscale updrafts C_{mu}, evaporation of condensate from mesoscale updrafts E_{me}, and evaporation in mesoscale downdrafts E_{md}. In addition, a transfer of liquid water C_A from the convective updrafts to the mesoscale anvils occurs. (To be definite, these quantities will all be defined as positive semidefinite.) Based on empirical study, Leary and Houze (1980) provide coefficients relating these quantities. The procedure by which their analysis is combined with the parameterization follows.

1) Evaporation and sublimation associated with convective updrafts and downdrafts

From the parameterization for cumulus updrafts in section 2a, C_u can be obtained directly ($\int_{p_t}^{p_b} (\overline{\Upsilon_1}^*$

$+ \overline{\Upsilon_3}^*)dp$). The parameterization also yields R_c directly, so Leary and Houze's (1980) coefficient relating these quantities need not be used. Since the sum $R_c + \int_0^{p_g}(E_{cd} + E_{ce})dp + C_A$ must yield C_u, the ratio of $[\int_0^{p_g}(E_{cd} + E_{ce})dp + C_A]$ to C_u is also determined by the parameterization for cumulus towers. The ratios of E_{ce}, E_{cd}, and C_A *among themselves* follow Leary and Houze (1980).

Leary and Houze (1980) did not deal with the ice phase, but it is allowed for in the parameterization. The phase change represented by E_{ce} is sublimation if freezing occurs in the associated cumulus updraft; otherwise, it is evaporation. Evaporation is always assumed for E_{cd}. However, a vertically integrated balance must hold between all processes generating ice and all processes generating either liquid or water vapor from ice. These will be treated later and allow for the presence of melting in the region of the mesoscale downdraft.

A uniform vertical distribution is assumed for E_{ce} in a thin layer near the top of the corresponding cumulus updraft ($p_{tl} \leq p \leq p_t + 5$ kPa, where $p_{tl} = p_t - 1$ kPa). (The cloud model has a resolution of 1 kPa. Since substantial flux convergences can occur in the thin layer just above p_t, which is the last level at which w^* is nonzero, p_{tl} will appear with some frequency in the parameterizations now under discussion.) For E_{cd}, the vertical distribution is uniform between p_{tl} and p_g. As noted above, little information is available at present on the vertical distribution of most of the processes discussed in this section; as a consequence, simple distributions, which produce reasonable agreement with observed forcing by cumulus ensembles, have been assumed. No attempt to optimize these choices formally with respect to observations has been made; rather, future study should focus on the physical mechanisms responsible for these vertical distributions.

Evaporation and sublimation in convective updrafts and downdrafts can be treated individually for each subensemble in a multimodal ensemble, but the transfer of condensed water (C_A) to the mesoscale anvil is summed over the ensemble.

The remaining processes involve primarily the mesoscale circulation and its interaction with the ensemble of cumulus elements.

2) WATER VAPOR REDISTRIBUTION BY MESOSCALE UPDRAFTS

It is evident that the mesoscale updrafts that occur in mesoscale anvils can advect water vapor. Further, results presented in section 3 will show that the parameterization predicts that convective updrafts can provide large sources of water vapor in the cloud-top region. As this water vapor is advected upward, it can change phase and contribute to latent heat release in the mesoscale updraft. Water vapor redistribution by advection in mesoscale updrafts will be treated as the sum of two processes, for simplicity. The first, which is treated in this subsection, is the redistribution of water vapor supplied by the cumulus updrafts *only*. Advection of water vapor present in the environment of the cumulus updrafts but not supplied by the updrafts is considered in the next subsection.

The source of water vapor provided by the convective updrafts is denoted by Q'_{mf} and is given by

$$Q'_{mf} = \begin{cases} 0, & \text{if } Q_{mf} < 0 \\ Q_{mf}, & \text{if } Q_{mf} \geq 0, \end{cases} \tag{11}$$

where

$$Q_{mf} = -\overline{\Upsilon_2}^* - \overline{\Upsilon_4}^* - \frac{\partial \overline{\omega' q'}}{\partial p}. \tag{12}$$

The base of the mesoscale updraft occurs at the pressure p_{zm} where the least penetrative cumulus cloud in an ensemble begins to supply water vapor to the large-scale flow, that is, where Q'_{mf} becomes nonzero. The top of the mesoscale updraft occurs at p_{ztm}, where

$$p_{ztm} = p_{tl}^{(d)} - 30 \text{ kPa}. \tag{13}$$

The superscript (d) refers to the most penetrative cumulus subensemble. (In cases of very deeply penetrative cumulus cells, p_{ztm} is restricted to 10 kPa, unless $p_{tl}^{(d)} < 10$ kPa, in which case $p_{ztm} = p_{tl}^{(d)} - 1$ kPa.) The water vapor source Q'_{mf} at pressure p contributes $\int_0^{\tau_m} Q'_{mf}(t)dt$ to the vertically averaged water vapor mixing ratio in the stratiform region over its lifetime τ_m. This water vapor is distributed uniformly in a region between p and $p + \int_0^{\tau_m} \omega_m dt$. The integral $\int_0^{\tau_m} \omega_m dt$ is taken to be 30 kPa, except in cases where this would spread water vapor to pressures less than p_{ztm}; in these cases, the integral is reduced so that water vapor is redistributed only to pressures greater than p_{ztm}. The large-scale water vapor mixing ratio is augmented by $\overline{q_1}(p)$ when the contributions from $Q'_{mf}(p)$ for pressures from p_{zm} to p_{ztm} are summed. The value of 18 hours chosen for τ_m as a typical lifetime for a mesoscale circulation follows Leary and Houze (1980).

This formulation spreads the water vapor originating in a subensemble of cumulus towers over about 30 kPa. For the sample applications discussed in section 3, this corresponds to mesoscale vertical velocities in the lower ranges quoted by Leary and Houze (1980) (between 0.1 and 0.2 m s^{-1}). Ackerman et al. (1988) estimated that a mesoscale vertical velocity around 0.03 m s^{-1} would enable local adiabatic cooling associated with mesoscale ascent to compensate radiative heating of a mesoscale anvil higher and colder than those in section 3 [anvil tops ~17 km at ~195 K in Ackerman et al. (1988); anvil tops ~10–11 km at ~230 K in section 3]. The tentative vertical velocities used here are thus greater than those required for local, mesoscale compensation of radiative heating. The vertical variation of anvil radiative heating could lead to larger

vertical velocities than required to compensate the mean radiative heating of the anvil. Ackerman et al.'s (1988) radiative heating rates are much greater in lower regions of the anvil; the resulting localized instability in the anvil could account for the larger vertical velocities. Thus, it seems at least possible that the dynamics of the mesoscale circulation are partially driven by the intense radiative forcing experienced by the stratiform anvil.

The *large-scale* water vapor tendency associated with the redistribution of water vapor having cumulus cells as it source is

$$\frac{\overline{q_l}(p)}{\tau_m} - Q'_{\text{mf}}.$$

The redistributed water vapor $\overline{q_l}$ accumulates in the mesoscale region, whose fractional area is denoted as a_m. Future study should focus on means for calculating a_m based on cumulonimbus outflow dynamics, but in the present application, Leary and Houze's (1980) result is used:

$$a_m = 5 \sum_{i=1}^{N} a_i(p_t). \tag{14}$$

(The summation is over N subensembles.) The redistributed water-vapor mixing ratio in the mesoscale anvil is then $\overline{q_l}/a_m$, which may exceed saturation and thereby change phase. This process is discussed in the next subsection.

3) Deposition in mesoscale updrafts

The mesoscale anvils are assumed to consist of ice, which is furnished by deposition from water vapor and by transfer C_A from the cumulus updrafts. The first source of deposited ice is provided by the redistribution of water vapor provided by cumulus updrafts, described in the preceding subsection. The rate of ice deposition by this process is

$$\frac{\overline{q_l}(p)}{a_m \tau_m} - \frac{q_s[T_m(p)]}{\tau_m},$$

where q_s denotes saturation mixing ratio and T_m refers to the temperature in the mesoscale updraft [1 K above $\bar{T}$, following Leary and Houze (1980)]. The preceding process deals only with water vapor supplied by the cumulus updrafts; additional deposition occurs as large-scale water vapor in the mesoscale region surrounding the updrafts is lifted by mesoscale ascent. This process is parameterized in terms of the water vapor mixing ratio at the base of the mesoscale region, which is conserved as it undergoes mesoscale ascent until deposition begins, when

$$\bar{q}(p_{zm}) + \frac{\bar{q}_l(p_{zm})}{2a_m} = q_s[T_m(p)].$$

Deposition then proceeds at a rate

$$\omega_m \frac{\partial q_s}{\partial p}.$$

(The factor of 2 averages the water vapor from the cumulus updrafts over τ_m.) The vertical distribution of the mesoscale vertical velocity is assumed to be parabolic in form between p_{zm} and p_{ztm} and satisfies the integral constraint discussed after (13).

Then C_{mu} is estimated as the sum of these two processes: 1) water vapor supplied to the mesoscale environment by the cumulus updrafts, which changes phase as it is lifted in the mesoscale anvil circulation and 2) water vapor in the mesoscale environment of the cumulus updrafts, which changes phase as the mesoscale anvil cloud of fractional area a_m is lifted at vertical pressure velocity ω_m.

4) Sublimation in mesoscale updrafts

The mechanisms that produce condensate in the mesoscale anvil, $\int_{p_{ztm}}^{p_{zm}} C_{mu}\,dp$ and C_A, can thus be calculated as described in the preceding two subsections and from the moisture budget of the cumulus updrafts, respectively. The sum of the rates at which condensate is provided to the mesoscale circulation by these two mechanisms must, over τ_m, be balanced by $\int_0^{p_g} (E_{me} + E_{md})dp + R_m$. The ratios of R_m, $\int_0^{p_g} E_{md}dp$, and $\int_0^{p_g} E_{me}dp$ to $\int_0^{p_g} C_{mu}dp + C_A$ are those of Leary and Houze (1980). However, since the latter is calculated directly, it is not necessary to impose a universal ratio between convective and mesoscale precipitation using Leary and Houze's (1980) ratio for R_m to R_c; rather, the relative role of mesoscale and convective processes can vary with the large-scale flow.

A uniform vertical distribution between p_{zm} and p_{ztm} is assumed for E_{me}.

5) Sublimation in mesoscale downdrafts

Sublimation in mesoscale downdrafts, E_{md}, is a relatively large component of the water budget of the mesoscale circulations associated with deep convection (Leary and Houze 1980). Rather than simply distribute E_{md} uniformly beneath the mesoscale anvil, a linear distribution decreasing with increasing pressure from p_{zm} is used:

$$E_{md}(p) = \begin{cases} 0, & \text{if } p < p_{zm} \\ \dfrac{2\left(\displaystyle\int_0^{p_g} E_{md}\,dp\right)(p_g - p)}{(p_g - p_{zm})^2}, & \text{if } p \geq p_{zm}. \end{cases} \tag{15}$$

The procedure for calculating $\int_0^{p_g} E_{md}dp$ is indicated in subsection 2b4. Since the mesoscale anvil is assumed to consist of ice, sublimation, rather than evaporation, occurs in the mesoscale downdraft.

6) MELTING AND FREEZING

Melting and freezing in an ensemble of cumulus updrafts without mesoscale structure was described in subsection 2a. Here a parameterization for melting and freezing in the presence of mesoscale circulations is presented. The calculations presented in section 3 show that the large-scale temperature tendencies produced directly by melting and freezing are small in magnitude; the chief effect of the ice phase is to add buoyancy to the relatively small volume occupied by cumulus updrafts at appropriate temperatures. This added buoyancy can change the structure of the cumulus ensemble enough to change significantly cumulus forcing of the large-scale flow as represented in (1) and (2). Thus, treatments of the vertical distributions of the large-scale effects of melting and freezing are crude here, but necessary balances between processes forming ice and removing ice are maintained.

Recalling that the anvil is treated as ice, condensate transferred thereto from the cumulus updrafts must either leave the updrafts as ice or freeze during transfer. In addition, as noted in subsection 2b1, E_{ce} proceeds by sublimation if $T^*(p_t) \leqslant 258$ K. Enough freezing must occur to provide this ice; the quantity of ice produced by the process described in subsection 2a can be either excessive or inadequate. For each subensemble individually, additional freezing or melting occurs to ensure this balance as follows.

If the sum of the vertical integral of freezing in the cumulus updraft $g^{-1}\int_{p_t}^{p_b}\bar{\Upsilon}^*_{5,\text{cell}}dp$ and the vertical integral of deposition in the cumulus updraft is less than C_A [or $C_A + g^{-1}\int_0^{p_g}\bar{E}_{ce}dp$, if $T^*(p_t) \leqslant 258$ K], additional freezing, $\bar{\Upsilon}^*_{5,m}$, occurs:

$$g^{-1}\int_0^{p_g}\bar{\Upsilon}^*_{5,m}dp = C_A \quad \text{if} \quad T^*(p_t) > 258 \text{ K}.$$

Otherwise,

$$= C_A + g^{-1}\int_0^{p_g}(\bar{E}_{ce} - \bar{\Upsilon}^*_3 - \bar{\Upsilon}^*_{5,\text{cell}})dp. \quad (16)$$

A uniform vertical distribution between p_{zm} and p_{ztm} is used for $\bar{\Upsilon}^*_{5,m}$; note that since this procedure is applied to each subensemble individually, each subensemble will have characteristic values of p_{zm} and p_{ztm}, unlike the case discussed in preceding subsections. Aggregate effects for the ensemble are obtained by summing the effects of the individual subensembles. The total freezing rate is

$$\overline{\Upsilon_5}^* = \bar{\Upsilon}^*_{5,\text{cell}} + \bar{\Upsilon}^*_{5,m}. \quad (17)$$

If $g^{-1}\int_{p_t}^{p_b}(\bar{\Upsilon}^*_{5,\text{cell}} + \bar{\Upsilon}^*_3)dp$ is greater than $C_A + \int_0^{p_g}\bar{E}_{ce}dp$, then melting occurs to ensure ice balance. The melting process discussed in subsection 2a in the absence of mesoscale effects is discarded and replaced by

$$g^{-1}\int_0^{p_g}\bar{\Upsilon}^*_6 dp = g^{-1}\int_0^{p_g}(\bar{\Upsilon}^*_{5,\text{cell}} + \bar{\Upsilon}^*_3 - \bar{E}_{ce})dp - C_A. \quad (18)$$

This melting is distributed uniformly between p_b and the pressure at which $\bar{T} = 273$ K.

Since mesoscale precipitation R_m reaches the surface as liquid in the cases treated in this paper, while originating as ice in the anvil, vertically integrated melting of magnitude R_m occurs, distributed uniformly between p_b and the pressure at which $\bar{T} = 273$ K. In situations where (16) holds, the melting of R_m is the only contributor to $\bar{\Upsilon}^*_6$; when (18) holds, the melting of R_m supplements that given by (18).

7) MESOSCALE EDDY FLUXES OF ENTROPY AND WATER VAPOR

The dynamics of the mesoscale circulations associated with deep convection are complex, as are the associated mesoscale fluxes of entropy and water vapor. As in treating the phase changes associated with these mesoscale circulations in the previous subsections, a semi-empirical approach is adopted. In general, mesoscale fluxes are calculated using (3), replacing a_i by a_m, where a_m is calculated using (14). The procedures for calculating the other terms in (3) are as follows.

Entropy and water vapor fluxes in mesoscale updrafts. In the region between p_{zm} and p_{ztm} (with reference to the complete cumulus ensemble, cf. section 2b2), the entropy and water vapor fluxes are calculated using the assumptions on T_m, q_m, and ω_m given in subsections 2b2 and 2b3.

Entropy and water vapor fluxes in mesoscale downdrafts. The magnitude of the vertical velocity ω_m in the mesoscale downdraft is constant (in units of pressure vertical velocity) between p_{md} and p_b, where

$$p_{md} = p_{zm} + 20 \text{ kPa}. \quad (19)$$

Its magnitude is half of the maximum magnitude of ω_m between p_{zm} and p_{ztm}. (No mesoscale vertical motion is assumed between p_{md} and p_{zm}.) To calculate the temperature and water vapor mixing ratio between p_{md} and p_b, the mesoscale eddy flux of moist static energy is assumed to vary from zero at p_{md} to a value equal to its minimum $(\overline{\omega' h'})_{\min}$ in the mesoscale updraft. To take rough account of the eddy fluxes associated with convective downdrafts, the total eddy flux is increased by 30% over the flux due to mesoscale motions.

[These assumptions are based on Leary and Houze (1980), especially their Fig. 7c.] Using

$$h'_m = c_p(T_m - \bar{T}) + L_1(q_m - \bar{q}), \quad (20)$$

T_m and q_m in the mesoscale downdraft can be calculated:

$$T_m - \bar{T} = \left\{ \frac{(p - p_{md})(\overline{\omega' h'})_{\min}}{(p_b - p_{md}) a_m \omega_m} - L_1 [r q_s(\bar{T}) - \bar{q}] \right\} \times \left[c_p + r L_1 \frac{\partial q_s(\bar{T})}{\partial T} \right]^{-1}, \quad (21)$$

$$q_m = r q_s(T_m). \quad (22)$$

The relative humidity r in the mesoscale downdraft varies linearly in p from 100% at p_{md} to 70% at p_b (cf. Table 3 in Leary and Houze 1980). The Clausius–Clapeyron equation is used to evaluate $\partial q_s / \partial T$. Equation (20) is obtained by expanding $q_s(T_m)$ in a Taylor series about $\bar{T}$, which enables h'_m in (19) to be expressed as a function of $T_m - \bar{T}$ only.

These profiles of mesoscale vertical velocity and mesoscale eddy flux of moist static energy imply that the corresponding fluxes of entropy and water vapor are nonzero at both p_{md} and p_b. These fluxes at p_b are applied to the planetary boundary layer ($p_b < p < p_g$), which is assumed to be well mixed, and these fluxes at p_{md} are applied to the region $p_{zm} < p < p_{md}$.

These preliminary solutions should be revised as more detailed knowledge of relevant physical processes develops. The formulation for mesoscale effects here is consistent with a conceptual sequence in which convective towers supply condensate and water vapor to provide an incipient mesoscale anvil. The mesoscale anvil further develops, at least partially in response to radiative heating, which triggers mesoscale ascent and additional condensation. Although physically consistent, this sequence introduces a problematic element in the practical issue of parameterization. Large-scale models in which cumulus parameterization is used have time steps far shorter than a day. The presence of mesoscale features, which still remain spatially subgrid, evidently requires that information regarding the point that a convective system has reached during its life cycle be carried in time as the large-scale model is integrated, that is, that cumulus parameterizations develop a "memory." Lacking this, an instantaneous parameterization can attempt only to represent the average behavior of the mesoscale effects over their lifetime; this approach has been adopted here.

3. Applications

The parameterizations developed in section 2 are applied in this section to mean trough profiles from GATE and KEP. Both of these thermodynamic profiles represent tropical maritime conditions characterized by deep convection. Large-scale forcing by convection differed appreciably between GATE and KEP, with maximum heating occurring around 60 kPa for GATE and around 45 kPa for KEP (Thompson et al. 1979). Since much of the convection important for climate occurs in the tropics, the ability of the parameterization to capture this variability between different large-scale settings in the tropics is important.

Observed thermodynamic data and diagnosed forcing for GATE and KEP are discussed in Thompson et al. (1979) and Reed and Recker (1971), respectively. Reed and Recker (1971) do not provide a surface sensible heat flux; this value was estimated here by using Reed and Recker's (1971) surface moisture flux and assuming the KEP Bowen ratio was identical to that for GATE.

a. Cumulus ensemble

This section will focus on the vertical structure of forcing associated with parameterized convective systems. Observed precipitation for the GATE and KEP profiles mentioned above will be used to close the parameterization. In model applications, the precipitation would need to be calculated using a parameterized closure. Use of observed precipitation permits an evaluation of details of vertical structure without the additional complication and uncertainty arising from the closure for the integrated intensity of the convective system.

An ensemble of cumulus cells is selected as follows. LeMone and Zipser (1980) presented distribution functions for the vertical velocities and updraft diameters of cumulus updraft cores observed during GATE. Their distributions for the height range from 4300 to 8100 m were used to construct an ensemble of clouds modeled using (5)–(7). The average vertical velocities in the model clouds in the height range from 4300 to 8100 m were used for comparison in this process. These vertical velocities are largely controlled by the value of $\beta / R(p_b)$ in (7). A value for $\beta / R(p_b)$ of 0.183×10^{-3} m^{-1} is consistent with other cumulus parameterizations (e.g., Anthes 1977) and observations of GATE cumulus radii by LeMone and Zipser (1980). For the GATE profiles, this value of $\beta / R(p_b)$ in (6) predicts an average vertical velocity in the specified height range of about 2.8 m s^{-1}. About 70% of the observed GATE updraft cores were weaker. These modeled cumulus updraft elements lost vertical momentum at 57 kPa. Since the cumulus parameterization is intended for deep convection, these updrafts were selected as the least penetrative members of the ensemble.

The relative numbers of other, more penetrative members of the ensemble were then constructed. Values of $\beta / R(p_b)$ were selected to produce cumulus elements whose vertical momentum vanished in successively higher vertical layers. (The resolution of these vertical layers was defined by the heights at which observations were available.) This process was continued until an element was constructed whose vertical velocity was sufficiently high that the cumulative frequency of weaker updraft cores reached 99%, based on LeMone and Zipser's (1980) observations. An addi-

tional, final member of the ensemble was selected so that its vertical momentum vanished around 20 kPa, near the observed maximum extent of penetration. Figure 1 illustrates the cumulative distribution functions of vertical velocity for both the modeled and observed ensembles. Liquid water contents ranged from 2.0 to 5.3 g kg^{-1} for the GATE ensemble, with the weakest members having the lowest contents. The KEP range was 2.4 to 6.2 g kg^{-1}. For updrafts studied in the Taiwan Area Mesoscale Experiment, which were characterized by vertical velocities similar to those in GATE, Jorgensen and LeMone (1989) reported maximum cloud liquid water contents around 0.5–1.0 g kg^{-1}, somewhat lower than those calculated for the most frequent members of the ensemble and considerably lower than those obtained for its strongest members.

Each member of the ensemble is governed by (5)–(7), and each subensemble requires an initial condition for a at p_b. (The initial conditions on temperature and vertical velocity are the same for all subensembles and were chosen as indicated in subsection 2a.) The *relative* fractional areas are calculated from

$$\frac{a_j}{a_i} = \frac{n_j R_j^2}{n_i R_i^2}, \tag{23}$$

where n_j/n_i is known by virtue of the procedure described in the preceding paragraph to construct the ensemble. The values for R_j/R_i are chosen such that the cumulative frequencies for n_j/n_i and R_j/R_i are the same for a given subensemble. Although Zipser and LeMone (1980) noted that the correlation between vertical velocity and radius was not particularly strong, this assumption is at least reasonably plausible physically. Finally, the actual values for the fractional areas at cloud base are obtained by requiring that the entire ensemble yield observed precipitation (when combined with precipitation from circulations outside of the cumulus updrafts). In prognostic applications, the relative mass fluxes could be required to sum to parameterized precipitation.

It may be noted that the right-hand side of (7) depends on $\sqrt{a}$. Thus, changes in the cumulus vertical velocity profiles occur for a specified value of $\beta/R(p_b)$ as $a(p_b)$ changes. However, these changes are quite small over the ranges of $a(p_b)$ encountered in these experiments ($\sim$0.02 m s^{-1}). This slight degree of nonuniqueness in the procedure could be eliminated by assuming the fractional rate of entrainment to be constant, rather than inversely proportional to cumulus radius.

Figure 2a shows the mass fluxes associated with some members of the ensemble for the GATE case. The absence of an observed frequency distribution for the KEP vertical velocities necessitated an arbitrary assumption to construct an ensemble for that case. The cumulative frequency for the KEP case where $\beta/R(p_b)$ takes the value 0.183×10^{-3} m^{-1} was chosen to be identical to the corresponding frequency for GATE. The resulting ratio of GATE vertical velocity to KEP vertical velocity was then assumed to hold for all other cumulative frequencies of the KEP ensemble. Figure 1 shows the cumulative frequency distribution for the KEP ensemble, and Fig. 2b illustrates the mass fluxes associated with some members of that ensemble.

For GATE and KEP, the maximum vertical velocities associated with most penetrative subensembles are about 10.3 m s^{-1} and 14.8 m s^{-1}, respectively. Although the GATE value is somewhat larger than the maximum average vertical velocities observed for updraft cores by LeMone and Zipser (1980), it agrees well with their highest maximum 1-s vertical velocities, and thus does not seem to be unreasonable, given its application to only 1% of the ensemble.

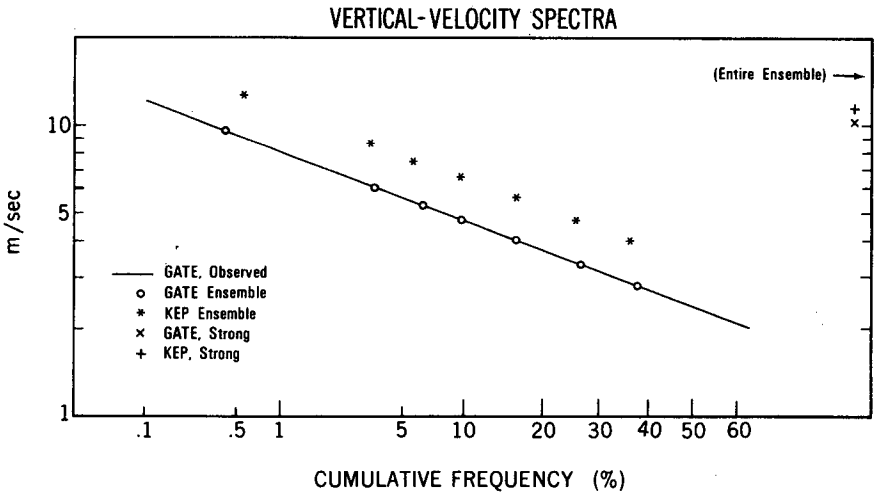

FIG. 1. Cumulative distributions for vertical velocity. Observations from LeMone and Zipser (1980). Strong cases described in text.

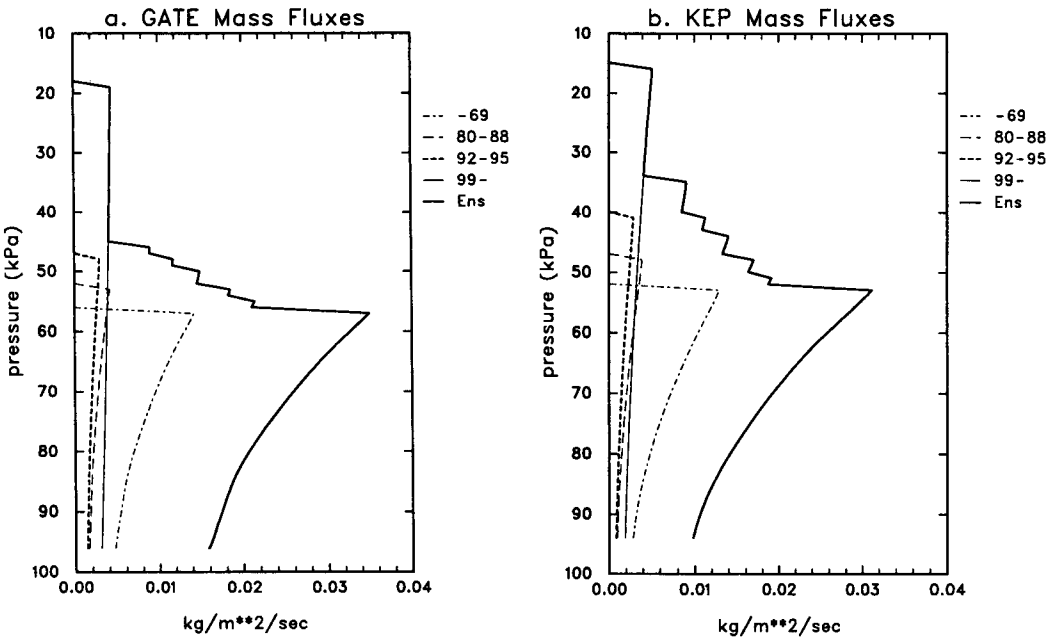

FIG. 2. Cumulus mass fluxes associated with selected subensembles for (a) GATE and (b) KEP. The curves are associated with ranges defined by the cumulative frequency of cumulus updrafts with weaker vertical velocities. "Ens" refers to the full ensemble.

b. *Large-scale forcing by cumulus updrafts*

Figures 3 and 4 show parameterized forcing by some members of the cumulus ensembles for GATE and KEP. (For clarity, surface fluxes have not been included in these figures, which show only the effects of the cumulus updrafts.) Thermal forcing consists of heating at nearly all heights, with the heating profiles attaining greater maxima with sharper peaks for the members of more limited penetration. Except for the most penetrating subensemble, which dries throughout, the moisture forcing consists of drying at low heights and

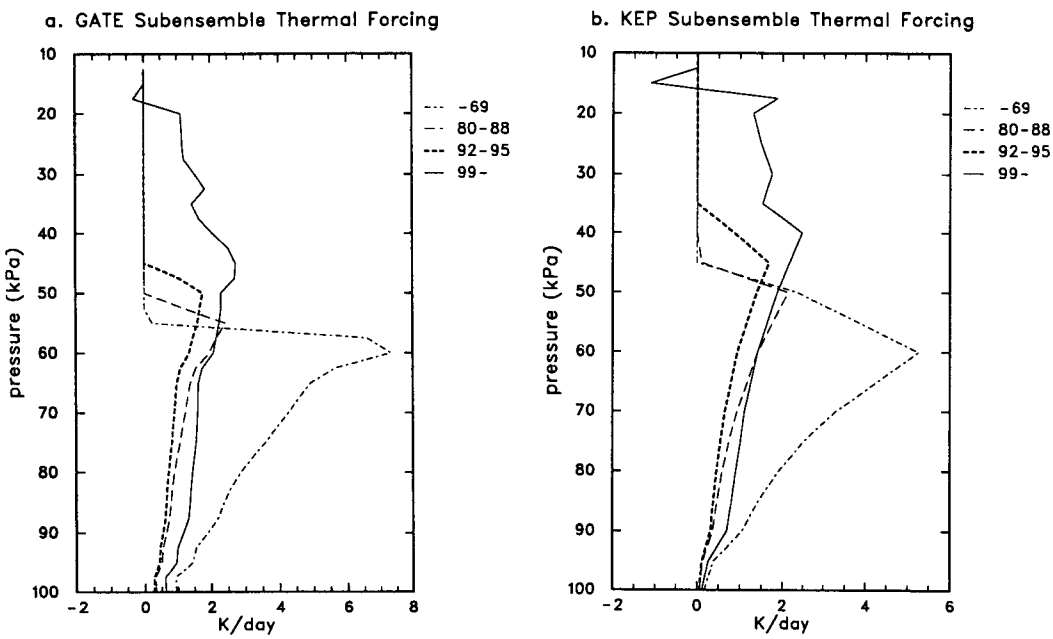

FIG. 3. Cumulus thermal forcing, $c_p^{-1} \sum_{i=1}^{6} L_i \overline{\Upsilon_i^*} - \pi^{-1} \partial \overline{\omega' \theta'} / \partial p$, by selected subensembles, denoted as in Fig. 2 for (a) GATE and (b) KEP. Surface fluxes are set to zero to isolate cumulus forcing.

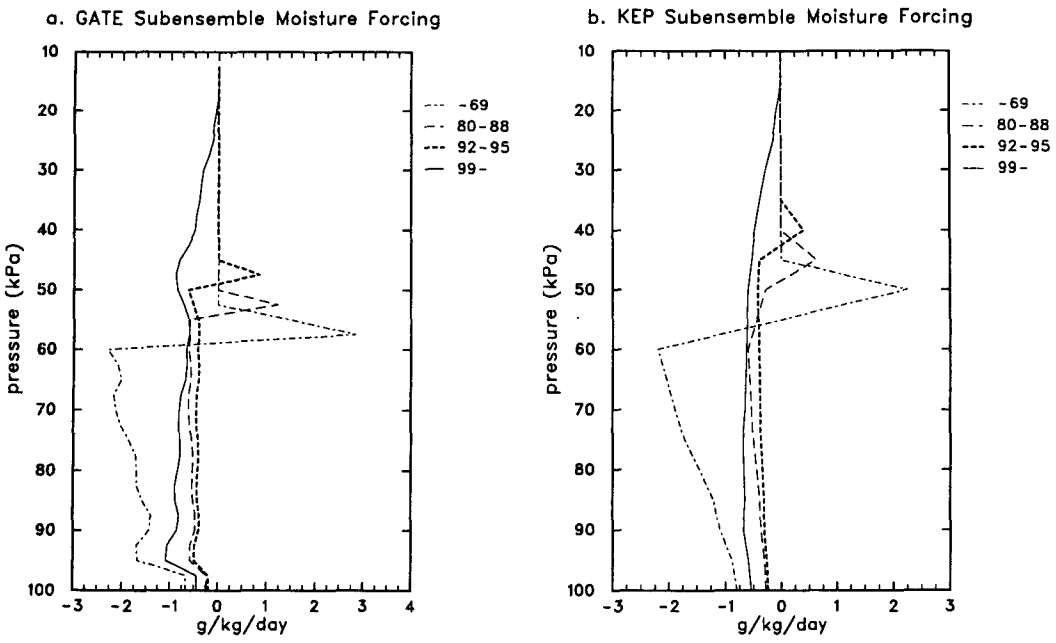

FIG. 4. As in Fig. 3 except for cumulus moisture forcing, $-\sum_{i=1}^{4}(|L_i|/L_i)\overline{\Upsilon_i^*} - (\partial\overline{\omega' q'}/\partial p)$.

moistening near the level of zero vertical momentum. This moistening is produced by convergence of cumulus-induced eddy fluxes of water vapor.

Cumulus temperatures are cold enough for freezing to occur in the convective updrafts in only the most penetrative 1% and 6% of the ensemble members for GATE and KEP, respectively. However, freezing is quite important in determining the penetrative extent of these elements. For example, the most penetrative GATE subensemble would have reached only 32 kPa without freezing, and would have reached only 28 kPa, even with no entrainment. The effect of freezing on the integrated intensity of the GATE ensembles is less dramatic; without freezing, precipitation is reduced by about 2% for GATE and about 4% for KEP.

The fractional areas occupied by the entire ensemble of updrafts at cloud base is 0.028 for GATE [in good agreement with a height-independent observational estimate for GATE of 0.025 by Leary and Houze (1980)] and 0.018 for KEP.

Figures 2–4 also illustrate that the most penetrative members of the ensemble contribute to mass fluxes, thermal forcing, and moisture forcing to a much larger extent than would be suggested by their frequency of occurrence; this is particularly evident with respect to the deepest 1%.

c. *Circulations outside cumulus updrafts*

Figure 5 shows the contributions to forcing by the circulations outside cumulus updrafts. Comparison of these figures with Figs. 3 and 4 shows that some of these processes are of sufficiently large magnitude to modify significantly forcing produced by the cumulus updrafts. Forcing associated with deposition in mesoscale updrafts, sublimation in mesoscale downdrafts, and mesoscale fluxes is large. (Thermal forcing associated with mesoscale eddy fluxes of entropy, not illustrated, has a vertical structure roughly like that for the corresponding moisture fluxes. It ranges from about -1 K day^{-1} in the planetary boundary layer to about 1 K day^{-1} in the upper troposphere for both GATE and KEP.) In the mesoscale updraft, the mesoscale fluxes remove entropy and moisture from the lower regions and add it to the upper regions. In the mesoscale downdraft, above the planetary boundary layer, entropy and moisture are added. However, when it reaches the planetary boundary layer, the mesoscale downdraft has become cooler and drier (with respect to specific humidity) than the large-scale flow, and the mesoscale downdraft acts to cool and dry the boundary layer. The mesoscale downdrafts are important components of the heat and moisture budgets in the boundary layer.

Averaged over the large scale, melting and freezing (not shown) are modest. For both GATE and KEP, the magnitude of the large-scale thermal forcing associated with these processes does not exceed 1 K day^{-1}.

d. *Combined forcing by cumulus updrafts and mesoscale circulations*

Figures 6 and 7 demonstrate forcing due to the combined effects of cumulus updrafts and the circulations outside the cumulus updrafts. Given the simple vertical

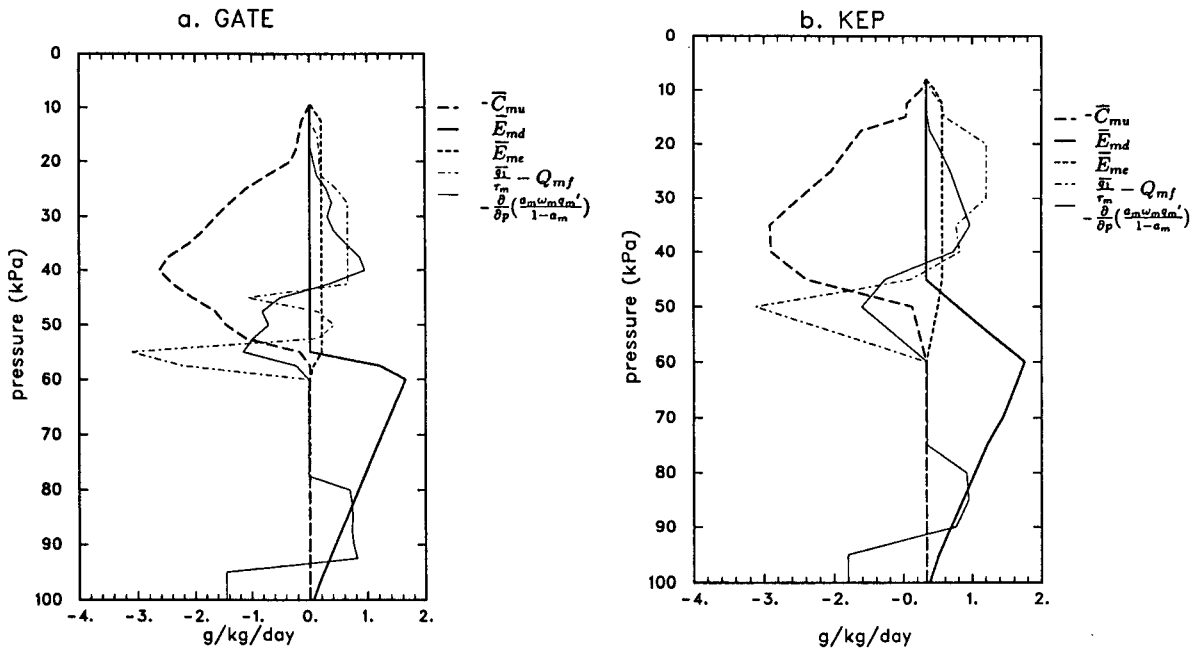

FIG. 5. Large-scale moisture tendencies associated with mesoscale processes for (a) GATE and (b) KEP.

distributions assumed for the latter, the overall agreement is reasonable for both thermal and moisture forcing. The calculations for an ensemble consisting only of cumulus updrafts use cumulus-base mass fluxes that yield the observed precipitation, with evaporation treated as described in section 2a. In these cases, the forcing illustrated is that which would be produced if an ensemble consisting only of cumulus updrafts were to produce the observed precipitation. Clearly, for GATE, the thermal forcing produced by an ensemble

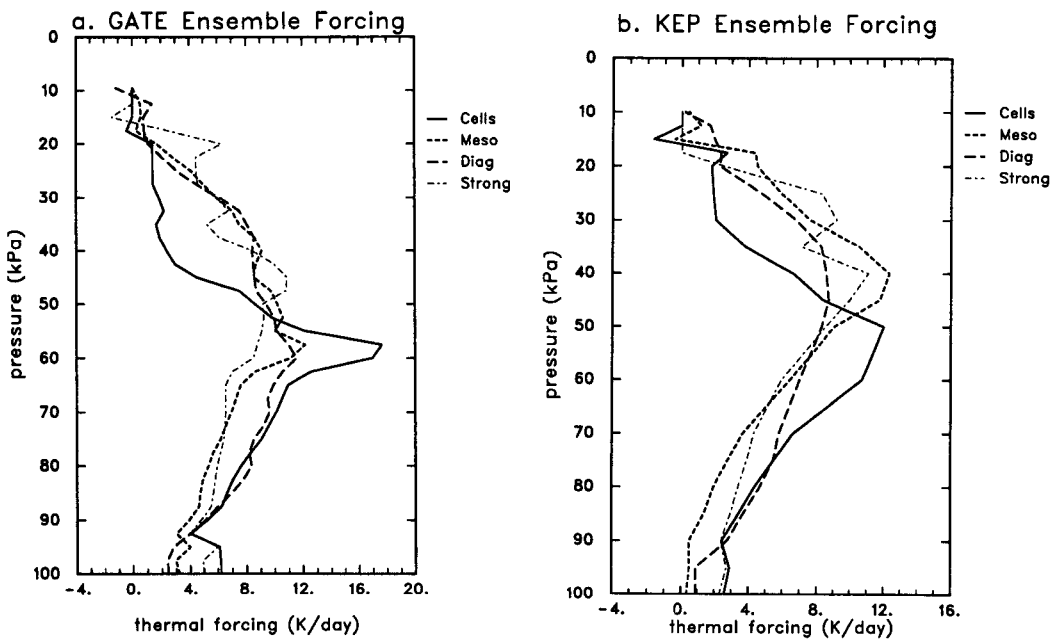

FIG. 6. Thermal forcing by cumulus ensembles for (a) GATE and (b) KEP. Cells: ensemble of cumulus updrafts only. Meso: ensemble of cumulus updrafts and circulations outside updrafts. Diag: diagnosed from field observations. Strong: monomodal ensemble, constructed as discussed in text.

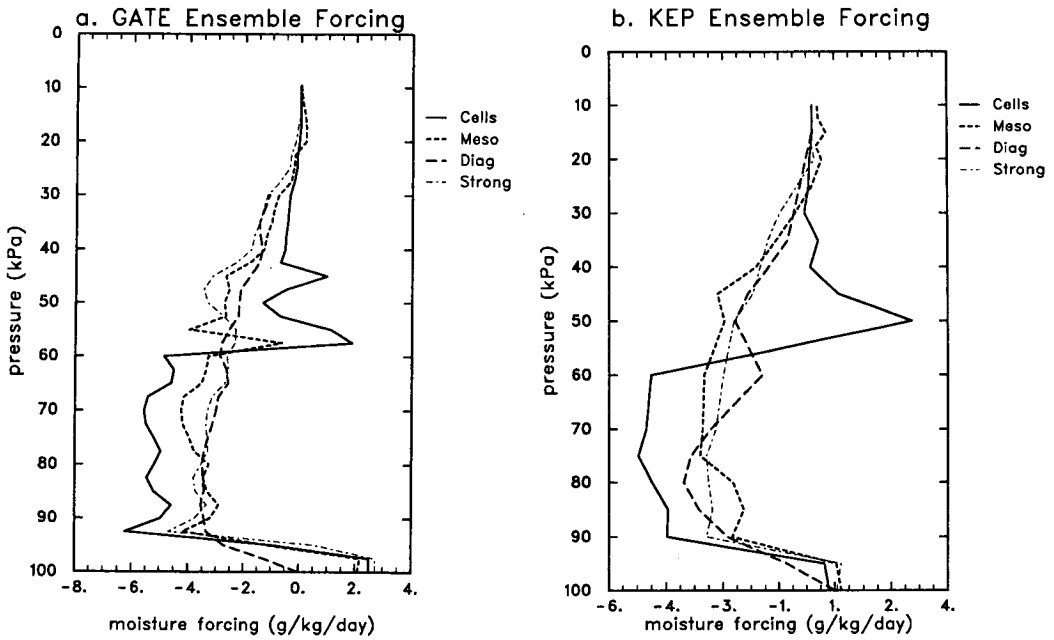

FIG. 7. As in Fig. 6 except for moisture forcing.

consisting only of updrafts produces a maximum in thermal forcing in significant excess of that diagnosed. In addition, for KEP, this maximum occurs at lower altitudes than diagnosed. Thermal forcing in the middle and upper troposphere is significantly less than diagnosed when only cumulus updrafts are considered. Without mesoscale circulations, parameterized moisture forcing exhibits excessive drying in the lower troposphere and produces an unobserved source of water vapor in the middle troposphere for both GATE and KEP.

Also illustrated in Figs. 6 and 7 is the forcing produced by a monomodal distribution of cumulus updrafts only. The vertical velocities for these cases ("strong") are indicated in Fig. 1. These cases are illustrated because they produce forcing in fair agreement with diagnosed forcing. However, as Fig. 1 shows, their vertical velocities are highly inconsistent with observations. Further, the liquid water contents associated with the "strong" cases peak around 5.5 g kg^{-1}, well above the limited observations reported by Jorgnesen and LeMone (1989) for cumulus updrafts. Consequently, any microphysical or radiative interactions depending on vertical velocity would be problematic. As examples, the maximum cloud fractional area for the GATE strong case is 2.8%, while for the case including GATE mesoscale effects it is 14%. The corresponding figures for KEP are 1.6% and 16%. Thus, for a cumulus parameterization to be useful in cloud–radiative interaction studies, more than just the mass fluxes must be considered. Satisfying constraints involving vertical momentum eliminates some solutions that are arguably reasonably acceptable (e.g., strong) if only thermal and moisture forcing are of interest.

While differences remain between parameterized and diagnosed forcing when mesoscale circulations are included, these differences are much smaller than those for the multimodal updrafts-only parameterization. With mesoscale effects, these differences consist mainly of inadequate parameterized thermal forcing in the lower troposphere; for KEP, the magnitude of the maximum is also overestimated. An underestimate in the entropy-flux convergence associated with the mesoscale and cumulus-scale downdrafts could be one reason for weak thermal forcing in the lower troposphere; the treatment of these downdrafts presented in section 2b is obviously preliminary and empirical in character. Also, shallow cumulus convection has not been treated, and the diagnosed forcing profiles are certainly subject to some uncertainty, if only due to the difficulty of estimating cloud radiative forcing, which is required to isolate the thermal forcing illustrated in these figures from the observed apparent heat source. [The observed precipitation used to close the parameterization for GATE was the value reported by Thompson et al. (1979), which agrees within 0.1 mm day^{-1} of the value obtained by integrating the apparent moisture sink after adding the surface moisture flux. For KEP, the integral method was used to obtain the observed precipitation; the resulting value is about 20% greater than the precipitation reported by Reed and Recker (1971). Further, the precipitation estimated

by integrating the apparent heat source with corrections for the surface heat flux and radiative cooling differs from the moisture-integral method by about 10% for GATE and 2% for KEP. These figures provide some indication of the uncertainty inherent in the observations themselves.]

Note in Fig. 7 that the thermal forcing in the planetary boundary layer agrees more closely with diagnosis when mesoscale circulations are present. Cumulus updrafts alone are unable to remove much of the sensible heat flux from the surface that converges in the boundary layer and can even heat the boundary layer somewhat if updraft-base parcels are colder than their environment. For both GATE and KEP, the latter situation existed. When mesoscale circulations are present, the mesoscale and cumulus-scale downdrafts both act to cool the boundary layer. Further, substantial precipitation is generated by the mesoscale circulation, so the mass fluxes at the bases of the convective updrafts required to produce the observed precipitation are less than when updrafts only are considered. There is therefore less heating of the boundary layer associated with cool parcels rising at the LCL. On the other hand, saturated cumulus-base parcels at the LCL remove water vapor from the boundary layer. The smaller upward mass fluxes at the LCL required when mesoscale effects are parameterized therefore reduces the drying of the planetary boundary layer and largely offsets (Fig. 7a) or even overrides (Fig. 7b) the drying produced by mesoscale downdrafts.

For GATE, the parameterized ratio of convective to mesoscale precipitation is 77%. [Leary and Houze (1980) estimated this ratio to be about 60%.] For KEP, only about 68% of the total precipitation was convective; that is, mesoscale circulations were relatively more important in the Pacific than in the east Atlantic. The implications for the vertical structure of the thermal forcing are significant. Diagnosed thermal forcing peaks at pressures about 15 kPa lower for KEP than for GATE (Fig. 6). As is evident from Fig. 6, a parameterized ensemble consisting only of cumulus updrafts is unable to produce fully this observed distinction, which is due in part to the larger relative role played by mesoscale circulations in KEP. Since the heating associated with the mesoscale circulations is strongly peaked in the upper troposphere (Fig. 5), convective systems in which mesoscale circulations are relatively more important are characterized by thermal forcing whose heating peaks at higher altitudes. The vertical velocities in the KEP cumulus ensemble are greater than those in the GATE ensemble, as is indicated by Fig. 1. (This is a consequence of differing stabilities in the large-scale soundings for GATE and KEP.) At higher vertical velocities, the ratio of cumulus rainfall to cumulus condensation is less, as a consequence of the dependence of the cumulus microphysics on w^*. For the GATE ensemble, this ratio is 73%, while for KEP it is only 60%. (Physically a cumulus parcel moves more quickly through a given pressure interval at high w^*, and the microphysical processes required to form rainwater have less time during which to act.) In KEP, there is thus more liquid available for the mesoscale anvil.

4. Discussion and concluding remarks

The parameterization developed and demonstrated in the preceding sections recognizes that both mass fluxes and vertical momentum dynamics are important to parameterizing cumulus updrafts. It is also based on the concept that to parameterize completely a convective system the mesoscale circulations associated with deep convection must also be considered. Knowledge of vertical momentum dynamics permits the use of more realistic microphysical formulations. The use of more realistic cumulus microphysics is related to the parameterization of mesoscale effects associated with deep convection, since an important component of the water budget for these mesoscale circulations is provided by the condensate not precipitated from the updrafts. The radiative properties of these mesoscale circulations are important controls on climate. Thus, there are compelling reasons to consider both mass flux and vertical momentum when parameterizing cumulus convection. In the context of the parameterization, cumulus updrafts whose vertical velocities and liquid water contents were realistic were unable by themselves to produce large-scale forcing that agreed with diagnoses; when mesoscale effects were added, the parameterization agreed reasonably with observations. However, some problems related to the parameterization remain to be addressed and are discussed briefly.

The treatment of mesoscale effects in the parameterization must be regarded as an interim procedure. In particular, the use of many empirical relationships between various components of the water budget and simple vertical distributions for the mesoscale processes should be modified. Treating the vertical momentum and microphysics of the cumulus updrafts provides a foundation on which to do so, since the supplies of liquid water and water vapor for the mesoscale anvil clouds are provided. Future studies should focus on quantitative aspects of the dynamics and the radiative heating of the anvils and associated mesoscale ascent and the characteristics of downdrafts driven by evaporation of condensate.

Related to the mesoscale effects associated with cumulus convection is the clear emergence of a time scale thereof that precludes the traditional linking of cumulus parameterizations solely to the instantaneous atmospheric state; that is, in the future, cumulus parameterizations will require a "memory" that will carry information about the stage of the tower–anvil life cycle across time steps. In such an approach, cumulus thermal forcing during early portions of the life cycle would

be more similar to that depicted for cells in Figs. 6 and 7, while later stages would evolve toward or even beyond the mesoscale cases in these figures. Diagnosed and parameterized forcing were compared here as averages over the lifetime of the convective system; in reality, both probably vary from early stages dominated by convective updrafts to later stages dominated by mesoscale anvils. Indeed, Frank and McBride (1989) diagnosed for GATE and the Australian Monsoon Experiment that maximum cumulus thermal forcing shifted upward as the system moved through its life cycle in accordance with this rough scenario.

Since the scale of mesoscale stratiform systems associated with cumulus convection is about 100 km (Leary and Houze 1980), very high resolution GCMs may be able to simulate mesoscale effects explicitly, once the parameterization for the cumulus updrafts is used. The parameterization for the updrafts can supply condensed water and water vapor, which could be acted upon by radiative transfer processes functionally dependent on liquid water content. The resulting radiative heating could be partly balanced by vertical motion in a manner consistent with the mesoscale mechanisms hypothesized here.

It is noted again that the present study has emphasized vertical structure (at the expense of closures for vertically integrated intensity). In prognostic applications, a closure for the vertically integrated intensity would be necessary. One possibility is the use of closures based on moisture convergence. Other closures, which have been used with mass-flux parameterizations, would also be candidates; in particular, for issues related to the mass flux associated with spectrum of clouds of differing entrainment, a well-established framework is provided by Arakawa and Schubert (1974). The merits and limitations of these closures are discussed in Emanuel and Raymond (1992). A major new issue associated with multimodal ensembles revolves around the formulation of such concepts as quasi-equilibrium of the cloud work function when a large fraction of cumulus forcing of the large-scale flow is actually due to mesoscale processes rather than convective cells.

In conclusion, this parameterization adds vertical momentum dynamics to mass fluxes to provide liquid water budgets for mesoscale anvil clouds, convective downdrafts, and radiative effects. Mesoscale effects introduce some difficult issues regarding time scales for convective systems relative to time steps in large-scale models and suggest that some problems in radiative transfer will need to be treated simultaneously with those of convection. The consideration of these effects provides a consistent framework for further experimental studies and parameterization development. These studies will be crucial to further development of GCMs. Adequate treatment of the mesoscale circulations will enhance not only the capability to represent vertical forcing distributions by convective systems but also cloud–radiative interactions that play a crucial role in climate.

Acknowledgments. GATE thermodynamic profiles and diagnosed forcing were provided by S. Payne (Naval Environmental Prediction Research Facility), and the corresponding KEP information was provided by R. Johnson (Colorado State University). General discussions on the cumulus parameterization problem with P. Rasch (NCAR) were helpful in developing some of concepts in this paper. I have also benefitted from discussions with V. Ramanathan (University of California) on radiative processes involving anvil clouds, D. Randall (Colorado State University) on convective destabilization of anvil clouds, M. LeMone (NCAR) and E. Zipser (Texas A&M) on diagnosis of cumulus forcing and GATE observations, and D. Perkey (Drexel University) on one-dimensional cumulus models. Computational resources were provided in part by a grant from the NCAR Scientific Computing Division. This project was supported by NSF Grant ATM-8807768 and the NCAR affiliate scientist program.

APPENDIX

Symbols and Units

Symbol	Description	Units
a	cloud fractional area	dimensionless
B	buoyancy	dimensionless
c_p	specific heat at constant pressure	J kg^{-1} K^{-1}
C_A	condensate transfer from cumulus updrafts to mesoscale circulation	kg m^{-2} s^{-1}
C_{mu}	deposition in mesoscale updraft	kg (water) kg^{-1} s^{-1}
C_u	vertical integral of condensation and deposition in cumulus updrafts	kg m^{-2} s^{-1}
e	vapor pressure	Pa
E_{cd}	evaporation in cumulus downdrafts	kg (water) kg^{-1} s^{-1}
E_{ce}	evaporation or sublimation from cumulus updrafts	kg (water) kg^{-1} s^{-1}
E_{md}	sublimation in mesoscale downdraft	kg (water) kg^{-1} s^{-1}

APPENDIX (*Continued*)

Symbol	Description	Units
E_{me}	sublimation from mesoscale updraft	kg (water) kg^{-1} s^{-1}
g	gravity constant	m s^{-2}
h	moist static energy	J kg^{-1}
L	generic latent heat	J kg^{-1}
L_1	latent heat of vaporization	J kg^{-1}
L_2	$-L_1$	J kg^{-1}
L_3	latent heat of sublimation	J kg^{-1}
L_4	$-L_3$	J kg^{-1}
L_5	latent heat of fusion	J kg^{-1}
L_6	$-L_5$	J kg^{-1}
n_i	number of cumulus elements in ith subensemble	dimensionless
p	pressure	Pa
q	vapor mixing ratio	kg (water) kg^{-1}
q_1	mixing-ratio augmentation by cumulus updrafts	kg (water) kg^{-1}
Q_{cw}	cloud water mixing ratio	kg (water) kg^{-1}
Q_{lw}	liquid water mixing ratio	kg (water) kg^{-1}
Q_{mf}	intermediate quantity for calculating Q'_{mf}	kg (water) kg^{-1}
Q'_{mf}	water vapor source from cumulus updrafts	kg (water) kg^{-1}
Q_{rw}	rainwater mixing ratio	kg (water) kg^{-1}
Q_r	radiative heating	J $kg^{-1}s^{-1}$
r	relative humidity	dimensionless
R	radius for cumulus updraft	m
R_c	precipitation from cumulus updrafts	kg m^{-2} s^{-1}
R_d	gas constant for dry air	J kg^{-1} K^{-1}
R_m	precipitation from mesoscale updraft	kg m^{-2} s^{-1}
R^*	cloud gas constant	J kg^{-1} K^{-1}
t	time	s
T	temperature	K
T_v	virtual temperature	K
$\mathbf{v}$	horizontal wind vector	m s^{-1}
w	vertical (geometric) velocity	m s^{-1}
z	geometric height	m
α	virtual mass coefficient	dimensionless
β	proportionality constant for entrainment	dimensionless
θ	potential temperature	K
μ	entrainment coefficient	m^{-1}
ρ	density	kg m^{-3}
τ_m	lifetime for mesoscale circulation	s
χ	generic property	variable
ϵ	ratio of molecular weights of water to dry air	dimensionless
ω	vertical (pressure) velocity	Pa s^{-1}
Υ_1	condensation rate	kg (water) kg^{-1} s^{-1}
Υ_2	evaporation rate	kg (water) kg^{-1} s^{-1}
Υ_3	deposition rate	kg (water) kg^{-1} s^{-1}
Υ_4	sublimation rate	kg (water) kg^{-1} s^{-1}
Υ_5	freezing rate	kg (water) kg^{-1} s^{-1}
Υ_6	melting rate	kg (water) kg^{-1} s^{-1}

The following apply generally:

- $(\ )_i$ refers to the ith subensemble.
- $(\ )_{i,j}$ refers to the ith phase transformation for the jth subensemble.
- $(\ )'$ refers to a departure from a large-scale average.
- $(\ )^*$ refers to a property or process in the convective system.
- $(\ )_b$ refers to the base of the cumulus updrafts.

$( )^e$ refers to a property or process in the cloud-free area.
$( )_g$ refers to the ground.
$( )_m$ refers to a property or process in the mesoscale circulation.
$( )_{md}$ refers to the top of the mesoscale downdraft.
$( )_o$ refers to 100 kPa.
$( )_s$ refers to saturation.
$( )_t$ refers to the top of the cumulus updrafts.
$( )_{tt}$ refers to the level 1 kPa above the top of the cumulus updrafts.
$( )_{zm}$ refers to the base of the mesoscale updraft.
$( )_{ztm}$ refers to the top of the mesoscale updraft.
$( )_{auto}$ refers to autoconversion.
$( )_{coll}$ refers to collection.
$( )_{cond}$ refers to condensation or deposition.
$( )_{ent}$ refers to entrainment.
$( )_{fall}$ refers to fallout.
$( )_{cell}$ refers to a process in the cumulus cells.
$( )_{min}$ refers to a minimum.
$( )^{(d)}$ refers to the most penetrative subensemble.
Δ refers to a finite change in the variable it precedes.

REFERENCES

Ackerman, T. P., K.-N. Liou, F. P. J. Valero, and L. Pfister, 1988: Heating rates in tropical anvils. *J. Atmos. Sci.*, **45,** 1606–1623.

Anthes, R. A., 1977: A cumulus parameterization scheme utilizing a one-dimensional cloud model. *Mon. Wea. Rev.*, **105,** 270–286.

Arakawa, A., and W. H. Schubert, 1974: Interaction of a cumulus cloud ensemble with the large-scale environment: Part I. *J. Atmos. Sci.*, **31,** 674–701.

Betts, A. K., 1986: A new convective adjustment scheme. I: Observational and theoretical basis. *Quart. J. Roy. Meteor. Soc.*, **112,** 677–692.

Cheng, M. D., 1989: Effects of downdrafts and mesoscale convective organization on the heat and moisture budgets of tropical cloud clusters. Part II: Effects of convective-scale downdrafts. *J. Atmos. Sci.*, **46,** 1540–1564.

——, and M. Yanai, 1989: Effects of downdrafts and mesoscale convective organization on the heat and moisture budgets of tropical cloud clusters. Part III: Effects of mesoscale convective organization. *J. Atmos. Sci.*, **46,** 1566–1588.

Donner, L. J., 1986: Sensitivity of the thermal balance in a general circulation model to a parameterization for cumulus convection with radiatively interactive clouds. *J. Atmos. Sci.*, **43,** 2277–2288.

——, H.-L. Kuo, and E. J. Pitcher, 1982: The significance of thermodynamic forcing by cumulus convection in a general circulation model. *J. Atmos. Sci.*, **39,** 2159–2181.

Emanuel, K. A., and D. J. Raymond, 1992: Report from a workshop on cumulus parameterization. *Bull. Amer. Meteor. Soc.*, **73,** 318–325.

Frank, W. M., and J. L. McBride, 1989: The vertical distribution of heating in AMEX and GATE cloud clusters. *J. Atmos. Sci.*, **46,** 3464–3478.

Fritsch, J. M., and C. F. Chappell, 1980: Numerical prediction of convectively driven mesoscale pressure systems. Part I: Convective parameterization. *J. Atmos. Sci.*, **37,** 1722–1733.

Houze, R. A., and A. K. Betts, 1981: Convection in GATE. *Rev. Geophys. Space Phys.*, **19,** 541–576.

Johnson, R. H., 1976: The role of convective-scale precipitation downdrafts in cumulus and synoptic-scale interactions. *J. Atmos. Sci.*, **33,** 1890–1910.

——, and G. S. Young, 1983: Heat and moisture budgets of tropical mesoscale anvil clouds. *J. Atmos. Sci.*, **40,** 2138–2147.

Jorgensen, D. P., and M. A. LeMone, 1989: Vertical velocity characteristics of oceanic convection. *J. Atmos. Sci.*, **46,** 621–640.

Kreitzberg, C. W., and D. J. Perkey, 1976: Release of potential instability. Part I: A sequential plume model within a hydrostatic primitive equation model. *J. Atmos. Sci.*, **33,** 456–475.

Kuo, H.-L., 1965: On formation and intensification of tropical cyclones through latent heat release by cumulus convection. *J. Atmos. Sci.*, **22,** 40–63.

——, 1974: Further studies of the influence of cumulus convection on large-scale flow. *J. Atmos. Sci.*, **31,** 1232–1240.

——, and W. H. Raymond, 1980: A quasi-one-dimensional cumulus cloud model and parameterization of cumulus heating and mixing effects. *Mon. Wea. Rev.*, **108,** 991–1009.

Leary, C. A., and R. A. Houze, Jr., 1980: The contribution of mesoscale motions to the mass and heat fluxes of an intense tropical convective system. *J. Atmos. Sci.*, **37,** 784–796.

LeMone, M. A., and E. J. Zipser, 1980: Cumulonimbus vertical velocity events in GATE. Part I: Diameter, intensity, and mass flux. *J. Atmos. Sci.*, **37,** 2444–2457.

Manabe, S., J. Smagorinsky, and R. F. Strickler, 1965: Simulated climatology of a general circulation model with hydrologic cycle. *Mon. Wea. Rev.*, **93,** 769–798.

Molinari, J., and T. Corsetti, 1985: Incorporation of cloud-scale and mesoscale downdrafts into a cumulus parameterization: Results of one- and three-dimensional integrations. *Mon. Wea. Rev.*, **113,** 485–501.

Reed, R. J., and E. E. Recker, 1971: Structure and properties of synoptic-scale wave disturbances in the equatorial western Pacific. *J. Atmos. Sci.*, **28,** 1117–1133.

Simpson, J., and V. Wiggert, 1969: Models of precipitating cumulus towers. *Mon. Wea. Rev.*, **97,** 471–489.

Thompson, R. M., S. W. Payne, E. E. Recker, and R. J. Reed, 1979: Structure and properties of synoptic-scale wave disturbances in the intertropical convergence zone of the eastern Atlantic. *J. Atmos. Sci.*, **36,** 53–72.

Tiedtke, M., 1989: A comprehensive mass flux scheme for cumulus parameterization in large-scale models. *Mon. Wea. Rev.*, **117,** 1779–1800.

Zipser, E. J., and M. A. LeMone, 1980: Cumulonimbus vertical velocity events in GATE. Part II: Synthesis and model core structure. *J. Atmos. Sci.*, **37,** 2458–2469.